THE INFLUENCE OF PARTICLE VIBRATING MOTION ON BED-LOAD VARIABLES

D. Rebai[1], A. Radice[1], and F. Ballio[1]

[1] Dept. of Civil and Environmental Engineering, Politecnico di Milano, Piazza L. da Vinci 32, 20133 Milano, Italy,

Corresponding author: D. Rebai (daniel.rebai@polimi.it)

Key Points:

- We distinguish "transport" (T) and "non-transport" (NT) states of particle motion and analyse them separately.
- The NT state involves isotropic vibrations, does not contribute to the sediment discharge but is significant for the kinetic energy budget.
- The mean number of moving particles and particle velocity change if NT movements are included in the sample

Abstract

The motion state of a particle is a crucial aspect in sediment transport problems. In this paper, we conceptualized three states: stillness, 'transport' and 'non-transport'. Starting from a data set of bed-load particle tracks obtained from Particle-Tracking-Velocimetry, we removed the bias from experimental uncertainty and applied one-dimensional, instantaneous and non-parametric criteria for distinguishing the different states. We present the

distributions of particle velocity for all the moving states and separating the transport and non-transport states, fitting a literature model to them. The transport state is related to isotropic particle vibrations and does not significantly contribute to the bed-load rate. Vice-versa, the choice of accounting or not accounting for the non-transport state has major quantitative impact on the mean number of moving particles and mean particle velocity. Finally, the non-transport state has non-negligible contribution to the total kinetic energy of the bed-load particles.

Plain Language Summary

Bed load is the transport of sediment particles in the vicinity of a channel bed. The transport of sediment by a turbulent flow has been widely studied in the last century. When the sediment transport rate is low, individual particles can be alternatively in motion or stillness. Quantitative determination of relevant quantities (number of moving particles, mean velocity, and others) may require a definition of criteria based on which a particle should be considered in motion or not at a certain instant (an issue that is far from being straightforward). Furthermore, particles can vibrate around fixed position, without an actual contribution to downstream transport. In this work, we proposed criteria for labelling stillness and motion states. The latter is further split into two states: 'transport' (associated with neat downstream motion) and 'non-transport' (associated with vibrations). Eventually, we characterized the properties of the states of motion and their contributions to global indicators of the bed-load process.

1 Introduction

The transition between two states – motion and rest – is one of the modelling keystones in bed-load processes, where it is common experimental evidence that particle motion is intermittent rather than continuous (Ancey et al., 2006). Furthermore, as discussed by, for example, (Furbish et al., 2012) and (Ballio et al., 2018), the sediment transport rate can be expressed either in a "flux form" or in an "entrainment form"; in the first case it is given by the product of a particle velocity and particle concentration, where both quantities are space-averaged (Kalinske, 1947) and, in the second case, by the product of a double-averaged entrainment rate and a mean hop length (Einstein, 1950). (Nikora et al., 2001, 2002) proposed three spatial and temporal ranges for bed-load motion: the local (between two successive collisions of a particle with the bed), intermediate (particle trajectories between two successive periods of rest), and global ranges (many intermediate trajectories). Many scholars focused their attention on studying bed-load kinematics at the intermediate trajectory scale (Lajeunesse et al., 2010; Liu et al., 2019; Roseberry et al., 2012), investigating hop length and duration or particle resting time. Finally, quantities related to single particle motion may be also used to derive others (entrainment and deposition rates, particle activity) that are commonly involved in mathematical models of the bed-load transport process (C. Ancey et al., 2008; Charru et al., 2004; Fan et al., 2016) . All the mentioned approaches require a clear definition of what stillness and motion are meant to be, as well as of the transition between the two states.

Bed load can be actually thought to comprise three particle states instead of two, splitting the state of motion into two different states. The first one is given by particles that, at a certain time, are displaced downstream (by saltation, rolling, or sliding); the second one corresponds to particles that vibrate around a certain position, without a neat displacement. Many names have been adopted for the vibrational state: "jiggle" (Wu et al., 2020), "rocking motion before the actual hop" (Liu et al., 2019), "shaking" particles (Shim & Duan, 2017), particles that "wiggled back and forth within their pockets" (Fathel et al., 2016), "rocking back and forth, or vibrating but not actively moving" (González et al., 2017), "wobbling but not moving" (Heays et al., 2014). Here, following (Salevan et al., 2017), we will distinguish two motion states for 'transport' (T) and 'non transport' (NT).

Several operational definitions of the transition between motion and rest have been proposed in the literature. Some of them are based on classifying particle's state based on a cut-off value that can be applied on one-dimensional (Heyman & Ancey, 2014; Lajeunesse et al., 2010; Roseberry et al., 2012), two-dimensional (Böhm et al., 2004;

Sechet & Le Guennec, 1999) or even three-dimensional (González et al., 2017) particle instantaneous velocity. Other definitions are based on properties of particle motions and rests over more than one instant: (Cecchetto et al., 2018), for example, prescribed a resting time greater than 0.1 seconds and a hop length greater than 1 grain diameter for a particle to be considered at rest or in a motion, respectively. (Martin et al., 2012) stated that "a resting particle was considered entrained when it moved a complete particle diameter, while a mobile particle was considered distrained when it failed to move more than one grain diameter within a second". (Liu et al., 2019) considered only "long particle trajectories, with integrated displacement over 10 d (here d is the particle size), and experiencing at least one step-stop-step sequence of motion and rest". In this context, reference was also made to second moments of particle position; for example, (Seizilles et al., 2014) labelled a particle as moving "if the standard deviation of its position over four successive pictures is larger than 0.1 d".

The definitions of motion and the experimental investigations cited above have been aimed at excluding NT motions, considering the vibrating particles as if they were at rest. Indeed, (Cecchetto et al., 2018; Liu et al., 2019) stated that their criteria of motion were adopted to exclude the non-transport particles; (Fathel et al., 2016) did not track the latter. By contrast, just few authors have focused on the NT state of particles. (Salevan et al., 2017) concluded that it is impossible to separate the T and NT states based on a threshold velocity and, therefore, proposed a mixed model for the probability density function (PDF) of the velocity accounting for both motion states. (Liu et al., 2019) also introduced three states: "moving" (similar to T), "active waiting" (NT) and "deep waiting" (stillness).

There is merit in studying the phenomenological properties of all motions (T and NT), as they may differently contribute to multiple facets of the bed-load process. However, the role of the NT state has not been clarified before. The research questions of the present manuscript are thus: (1) which are the kinematic properties of the non-transport state of particle motion? (2) Which is the impact of the NT state on variables commonly used in sediment transport problems? As already highlighted above, answering these questions requires a preliminary definition of how one should distinguish T and NT. Therefore, we also present criteria for labelling a particle state at any sampling time during the process. The analysis is anchored to particle tracks from an earlier experimental campaign with weak bed load.

2 Experimental set-up and Methods

The experiments analysed in this manuscript were carried out by (Campagnol et al., 2013) at the Hydraulics Laboratory of the Politecnico di Milano, employing a pressurized duct (5.80 m long, 0.40 m wide, 0.11 m high). In the downstream part of the flume, a recess section (2 m long and 0.4 m deep) was filled with Polybutylene Terephthalate (PBT) quasi-spheres with an equivalent diameter $d = 3\,\mathrm{mm}$ and a density $\rho_s = 1270\ \mathrm{kg/m^3}$. The same particles were glued on a series of plates positioned in the upstream reach (3.80 m long). A detailed description of the experimental set-up can be found in (Campagnol, 2012; Campagnol et al., 2015). In this work we use the results of three experiments performed at $u_*/u_{*c} = 1.11, 1.22$ and 1.30 (u_* is the shear velocity of the flow and u_{*c} is its threshold value for bed load).

Bed-load particle motion was investigated using Particle Tracking Velocimetry (PTV) after taking videos with a digital camera (frame resolution and rate were 970 × 700 pixel and 32 fps, respectively). The framed area had a stream-wise length of 49.8 cm and a transverse one of 36.5 cm; the duration of the videos was approximately 50 s.

The sediment was a mixture of black and white particles (95% and 5%, respectively) and only the white ones were tracked. We measured particle trajectories using the Streams Software (Nokes, 2012) following procedures already implemented by (Radice et al., 2017). After background removal, we converted grayscale frames into binary images using a single threshold monochrome algorithm: threshold intensity was fixed at 45 (out of 255); in addition, we set thresholds for minimum and maximum diameter of particle spots in binary images at 1.5 and 4.5 mm (the range was quite large compared to *d* because variable spot sizes could be obtained based on how light was reflected by any particle). Then, particle tracks were obtained using a two-dimensional search algorithm with global optimization; the searching window for a particle displacement within 1/32 s was ± 20 [mm] and ± 10 [mm] in the stream-wise and transverse directions, respectively.

3 Framework for Analysis

3.1 Conceptual definition of motion states

In the present study, attention is restricted to flows that are one-dimensional on average. However, transverse motion is also possible and thus we take x and y as the stream-wise and transverse coordinates, respectively. During a small

time interval δt, a particle performs a displacement with components $\delta x(t) = x(t) - x(t - \delta t)$ and $\delta y(t) = y(t) - y(t - \delta t)$, and magnitude $\delta r(t) = \sqrt{(\delta x(t))^2 + (\delta y(t))^2}$. The quasi-instantaneous (i.e., mean within δt) velocity components in the stream-wise and transverse directions are $u(t) = \delta x(t)/\delta t$ and $v(t) = \delta y(t)/\delta t$; the velocity magnitude is $V(t) = \sqrt{u^2(t) + v^2(t)}$. Finally, the components of the quasi-instantaneous particle acceleration are $a_x(t) = [u(t) - u(t - \delta t)]/\delta t$ and $a_y(t) = [v(t) - v(t - \delta t)]/\delta t$.

At any time, a particle may be in three states, namely stillness, T state of motion, NT state of motion. In Fig. 1 we show an idealized global trajectory. A particle is said to be at rest, at time t, if its absolute displacement is null (in green), whereas it is moving if the absolute displacement is different from zero (red and blue). Furthermore, a moving particle is said to be in T state if, at time t, it occupies an x position that has never occupied previously while moving downstream, otherwise its motion state is labelled as NT. In Fig. 1 states T and NT are depicted in red and blue, respectively. The total stream-wise distance travelled in T state of motion equals the total stream-wise distance travelled by the particle.

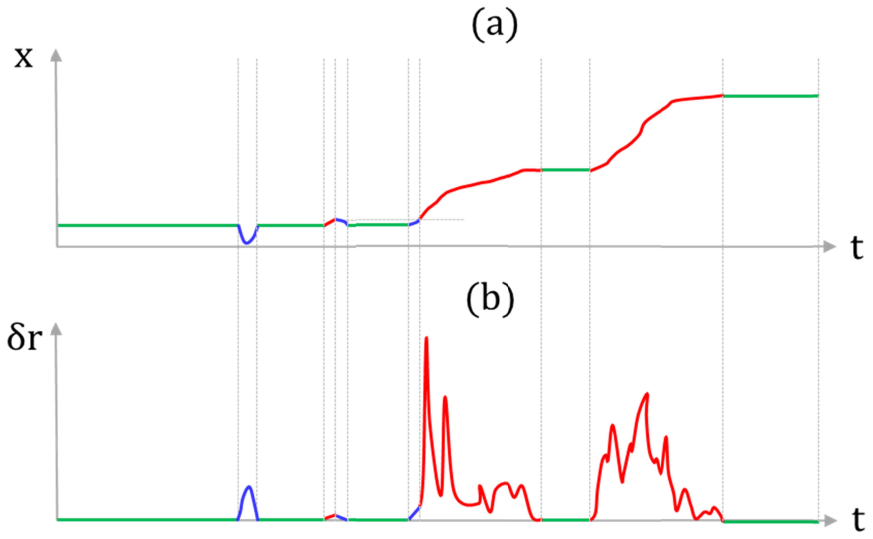

Fig. 1. Example of a particle trajectory: temporal evolution of (a) stream-wise position and (b) absolute displacement δr between two frames. Lines are coloured according to particle states: at rest (green); state T (red); state NT (blue). Definitions for the states are provided in the following.

3.2 Operational isssues

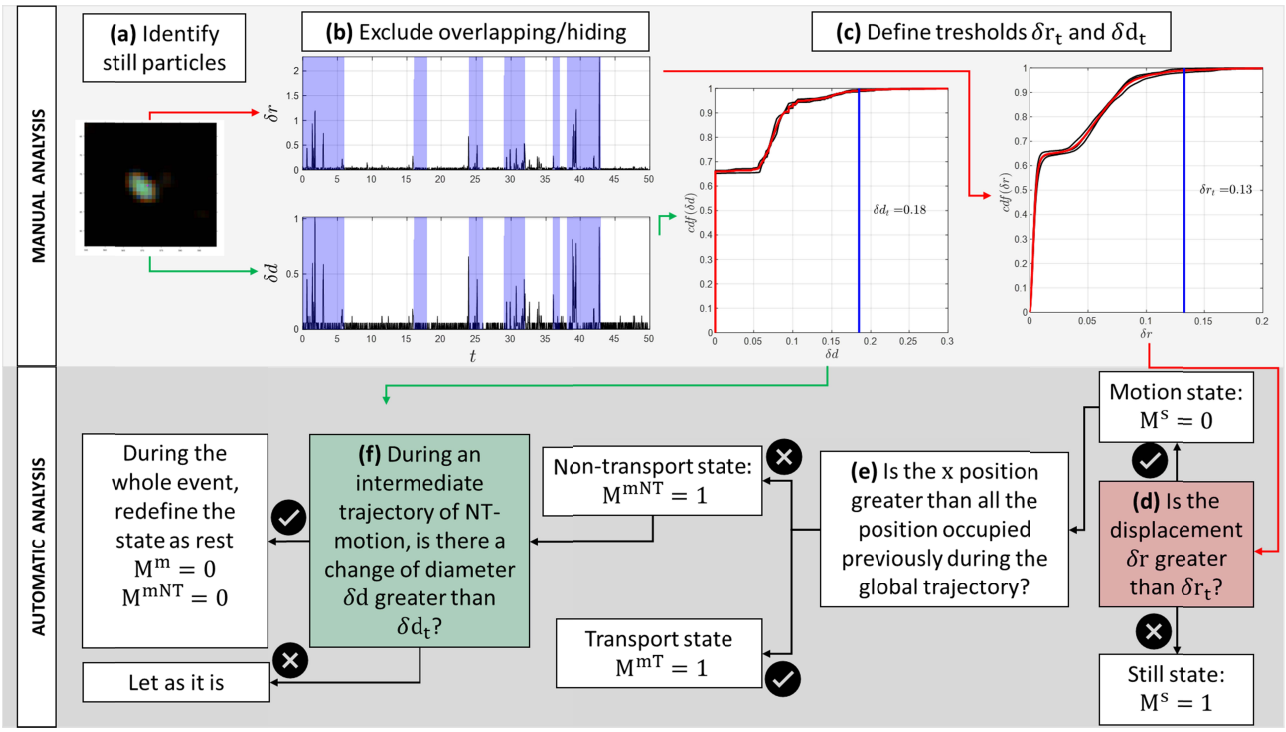

Fig. 2. Schematic representation of the algorithm used for state's labelling.

In Fig. 2 we summarize the algorithm used for labelling the state of a particle, starting from the analysis of experimental uncertainty.

In principle, one could apply the conceptual definitions described above to the tracks obtained with Streams; however, not all the displacements measured by the software corresponded to real ones. Any variation of the shape of a particle spot in a frame caused a corresponding variation of the position of the particle centroid, resulting in a displacement detected by the PTV algorithm. There were two main causes for this error: 1) small changes of light intensity produces a deformation of the particle; 2) the spot of another particle could partially hide (in case of a black one) that of a white still particle or overlap with it (in case of a white one) when they became sufficiently close to each other, resulting in a misattribution of NT state of motion to a still particle.

To address these problems, for each experiment we first manually selected 30 particles remaining still along a movie and analysed the corresponding time series of images; this allowed us to objectively determine proper filters for identifying potential erroneous movements (Fig. 2(a-c)). Then, these filters were automatically applied to all

identified particles, allowing to separate stillness from motion (Fig. 2(d-f)). Furthermore, for the time series of images the still particles (Fig. 2(a)) we excluded all the instants where we detected overlap with a white particle or hiding by a black particle (shaded area in Fig. 2(b)). In this way, we built a sample of data for particles that a human eye would soundly consider still while watching a movie. To overcome the first issue above (particle deformation due to changes of intensity, with consequent displacement of its centroid), we computed the frequency distribution function of displacements for these still particles: for the three experiments the distributions (Fig. 2(c)) were similar and, merging the three data sets, 99% of the displacements were smaller than $0.13\ \mathrm{mm}$. Therefore, $\delta r_t = 0.13\ \mathrm{mm}$ was taken as the minimum measurable displacement; displacements lower than this threshold were considered to be actually null, with the particle in a state of stillness. Concerning the second issue (particle hiding or overlap), we considered the same sample mentioned above, and computed the frequency distribution of the diameter change δd (Fig. 2(c)). Distributions for the three experiments were again similar and, for the experiments together, 99% of the change values were smaller that $\delta d_t = 0.18\ \mathrm{mm}$. Any diameter change greater than δd_t was thus reasonably attributed to a crossing. The measured centroid's position before and after hiding/overlapping issue is the same, mimicking a NT state trajectory; for this reason, motions previously labelled as in NT state were taken back to stillness if they presented spot size changes larger than δd_t.

3.3 Clipping functions

Based on the conceptual and operational considerations above, the recognition/labelling of a particle state was based on the following clipping functions (as described in Fig. 2(d) and 2(e)): $M^s(i,t)$ was used to recognize stillness based on a minimum displacement (i is a particle counter);

$$M^s(i,t) = \begin{cases} 1, & \delta r(t) \le \delta r_t \\ 0, & \delta r(t) > \delta r_t \end{cases} \quad (1)$$

while $M^{mT}(i,t)$ was used for the T state of motion based on a position criterion, mirroring that proposed by (Campagnol et al., 2013):

$$M^{mT}(i,t) = \begin{cases} 1, & x(t) > \max\limits_{0 \le \tau < t}[x(\tau)] \\ 0, & x(t) \le \max\limits_{0 \le \tau < t}[x(\tau)] \end{cases} \quad (2)$$

167

168 Finally, a function $M^{mNT}(i,t)$ was used for the NT state of motion. Given that, at any time, a particle can occupy
169 only one of the three states, it follows that $M^{mNT}(i,t) = 1 - M^{mT}(i,t) - M^{s}(i,t)$. As said, after applying (1) and
170 (2), some NT motion events were turned into stillness event if excessive variation ($\delta d(t) > \delta d_t$) of particle diameter
171 was observed (Fig. 2(f)).

172 We also introduced a clipping function, that will be used to obtain the sediment transport rate, to label particle
173 crossings of a transverse line. Considering a time interval δt, the sediment transport rate through a transverse line at
174 time t was computed starting from the volume of sediment crossing the line during the time period from $t - \delta t$ and t
175 (Ballio et al., 2014). Thus, for a reference transverse line with $x = x^*$, the clipping function $M_Q(i,t)$ stated whether
176 an i-th particles crossed the line and if it crossed it moving forwards or backwards during the time interval $[t -$
177 $\delta t, t]$:

$$M_Q(i,t) = \begin{cases} +1, & x(t-\delta t) \le x^*, \ x(t) > x^* \\ -1, & x(t-\delta t) \ge x^*, \ x(t) < x^* \\ 0, & \text{otherwise} \end{cases} \quad (3)$$

178 ## 3.4 Definition of motion variables

179 Expressions are provided here for some Eulerian variables commonly used in bed-load modelling. Let $N(t)$ be the
180 total number of particles in the framed area at time t, $N^{m}(t)$ the number of moving particles, $N^{mT}(t)$ the number of
181 particles moving with state T, and $N^{mNT}(t)$ the number of those moving with state NT. In this work, the variables
182 were determined as follows:

$$\begin{cases} N^{m}(t) = \sum_{i=1}^{N(t)} (1 - M^{s}(i,t)) = \sum_{i=1}^{N(t)} [M^{mT}(i,t) + M^{mNT}(i,t)] \\ N^{mT}(t) = \sum_{i=1}^{N(t)} M^{mT}(i,t) \\ N^{mNT}(t) = \sum_{i=1}^{N(t)} M^{mNT}(i,t) \end{cases} \quad (4)$$

183 Furthermore, the total number of particles that crossed the transverse line at $x = x^*$ at time t is given by

$$N_Q(t) = \sum_{i=1}^{N} M_Q(i,t)\left(1 - M^{s}(i,t)\right) = \sum_{i=1}^{N} M_Q(i,t)[M^{mT}(i,t) + M^{mNT}(i,t)] \quad (5)$$

184 We can also further subdivide $N_Q(t)$ based on the two states T and NT using the following equations:

$$\begin{cases} N_Q^{T}(t) = \sum_{i=1}^{N(t)} M_Q(i,t) M^{mT}(i,t) \\ N_Q^{NT}(t) = \sum_{i=1}^{N(t)} M_Q(i,t) M^{mNT}(i,t) \end{cases} \quad (6)$$

185 Eventually, we introduce the sediment kinetic energy per unit mass, k, which can also be decomposed in the
186 contributions of the T and NT states:

$$\begin{cases} k(t) = \frac{1}{2}\sum_{i=1}^{N(t)} V(i,t)^2\left(1 - M^{s}(i,t)\right) = \frac{1}{2}\sum_{i=1}^{N(t)} V(i,t)^2[M^{mT}(i,t) + M^{mNT}(i,t)] \\ k^{T}(t) = \frac{1}{2}\sum_{i=1}^{N(t)} V(i,t)^2 M^{mT}(i,t) \\ k^{NT}(t) = \frac{1}{2}\sum_{i=1}^{N(t)} V(i,t)^2 M^{mNT}(i,t) \end{cases} \quad (7)$$

187 After defining relevant variables, one can quantify how their determination depends on the operational criteria above
188 described. For example, Fig. 3 shows the effect of the filters δr_t and δd_t on the number of moving particles (we
189 show the time series) and the particle stream-wise velocity (we represent the histogram). In magenta, we depict the
190 results considering a particle in motion if its absolute displacement is non-null. In red, we show the results using (1)
191 to separate motion and stillness: the number of moving particles decreases by one order of magnitude and the central
192 peak of the velocity histogram is strongly reduced. Then, we also apply the filter on the change of diameter δd_t,

obtaining the blue curve: the number of moving particles is further reduced, and many negative velocities are removed.

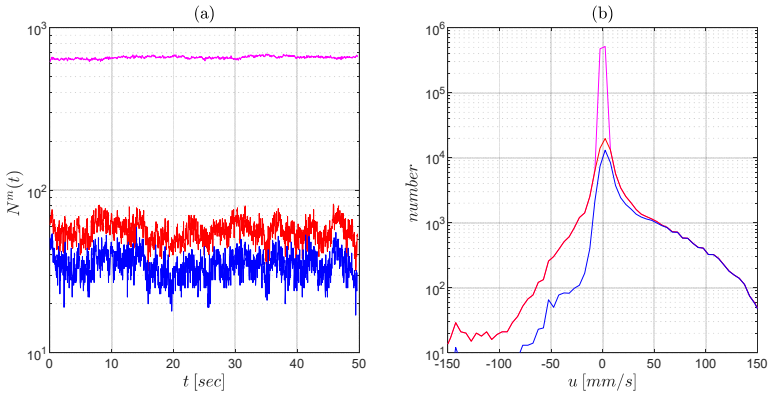

Fig. 3. (a) Time series of N^m; (b) Histogram of the quasi-instantaneous stream-wise velocity u. Without any filter: $\delta r_t = 0$; $\delta d_t = \infty$ (magenta). With the small displacement filter only: $\delta r_t = 0.13$ mm; $\delta d_t = \infty$ (red). With both filters: $\delta r_t = 0.13$ mm; $\delta d_t = 0.18$ mm (blue). Both panels refer to $u_*/u_{*c} = 1.22$.

4 Results and discussion

4.1 Separation among states of motion

As stated above, the first objective of this paper is the separation of two different particle motion states: T, causing net mass transport, and NT, for particle vibrations around a fixed position. Some preliminary results are depicted to check how our criteria separated the data and met the objective. Fig. 4(a) shows the cumulative number of particles crossing a line placed at mid-length of the investigation area, that represents a cumulative volume of transport sediment: the sediment transport is, indeed, almost entirely due to the T state, while the contribution of the NT state is negligible. Fig. 4(b) shows the instantaneous value of N_Q: the contribution of T (red) is always positive, while the one of NT (blue) can be either positive or negative. Considering NT, one could expect a cumulative null value; in our case the net contribution to solid flowrate is negative: we explain this finding considering that a backwards velocity is naturally appropriate for a motion in NT state, while it is less straightforward to separate forward motions.

Fig. 4(c) and (d) show results for the particle kinematics in NT state. Particles in NT state do not have a preferential direction of motion while they jiggle, as the PDFs of the instantaneous stream-wise and transverse velocity components are similar to each other (Fig. 3(b)); the distribution of u for the NT state is skewed towards negative values, reflecting the negative contribution to the sediment transport rate spotted in Fig. 4(a). The distribution of the quasi-instantaneous acceleration (Fig. 4(d)) also shows no preferential direction.

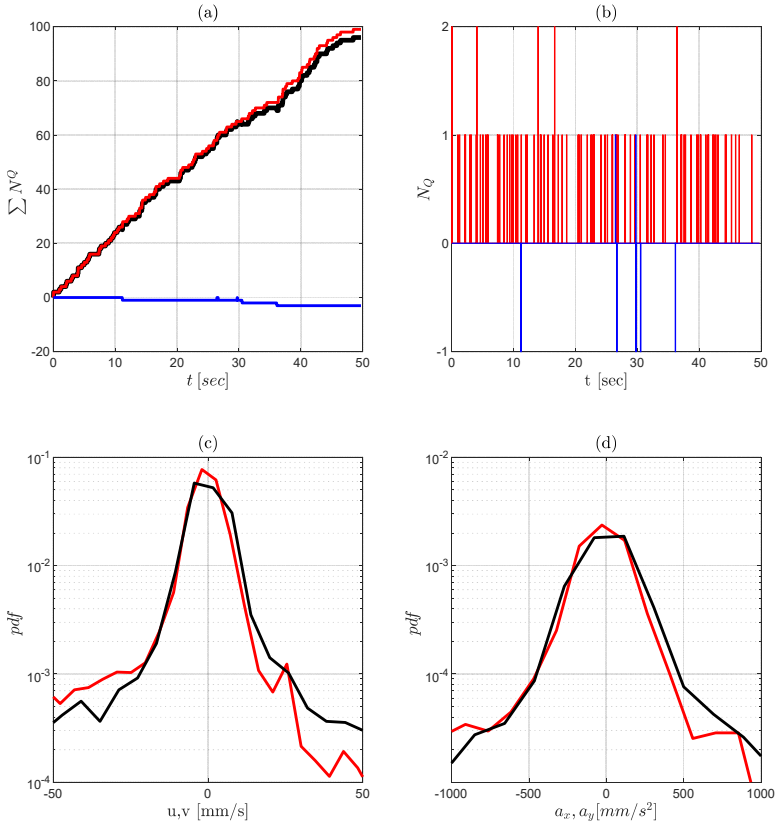

Fig. 4 (a) Cumulative number of particles crossing a line: all motions (black), NT state (blue) and T state (red). (b) Number of particles crossing a line: NT state (blue) and T state (red). (c) Observed probability distribution function of: u^{NT} (red); v^{NT} (black). (d) Observed probability distribution function of a_x^{NT} (red); a_y^{NT} (black). The panels refer to $u_*/u_{*c} = 1.30$.

4.2 Instantaneous stream-wise particle velocity

In Fig. 5 we show the histograms of the quasi-instantaneous stream-wise particle velocity. All of them present a clear peak around zero and are positively skewed to the right. Because of our definitions, all the negative velocities

226 are attributed to the particles in NT state; furthermore, particles in this state jiggle around a fixed position, thus the
227 corresponding motion velocities have a positive counterpart of the negative ones, resulting in an almost symmetric
228 histogram. On the other hand, the T state is obviously characterized by positive velocities, with a right tail of the
229 histogram much longer than that of the particle velocity in NT state; the mode of the distribution is at the lowest
230 values.

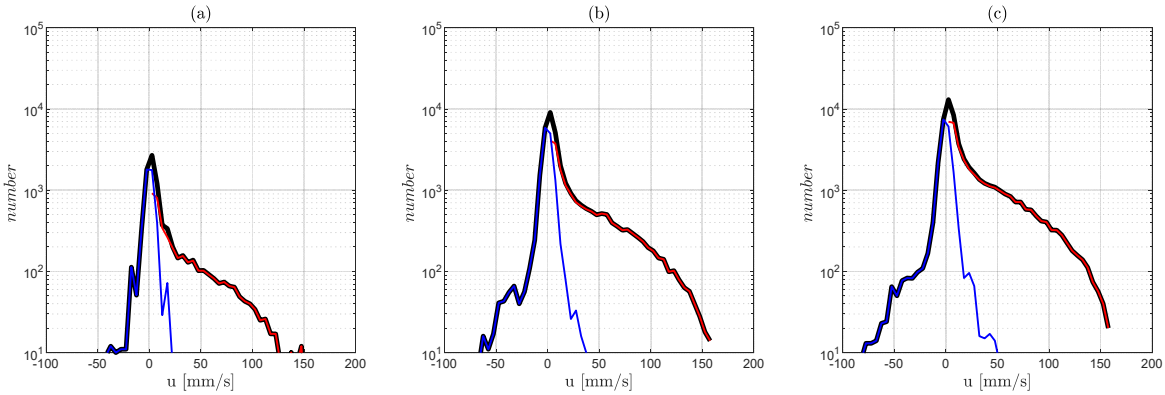

231
232 **Fig. 5.** Histograms of the instantaneous stream-wise velocity u: (a) $u_*/u_{*c} = 1.11$; (b) $u_*/u_{*c} = 1.22$ (c)
233 $u_*/u_{*c} = 1.30$. In all the panels: all motions (black), NT state (blue) and T state (red).

234 ## 4.3 Comparison of particle velocity distribution with a literature model

235 In Fig. 6 we depict the observed PDFs of a dimensionless particle velocity obtained using the characteristic settling
236 velocity, $V_s = \sqrt{g\Delta d}$ (where g is the gravitational acceleration, $\Delta = (\rho_s - \rho)/\rho$) and ρ is water density), as a
237 scaling factor, following (Lajeunesse et al., 2010). The PDF of the instantaneous particle velocity has been widely
238 studied in the literature, with most of the studies focused on the PDF of u^T. The latter has been proposed to follow
239 an exponential (Fathel et al., 2016; González et al., 2017; Lajeunesse et al., 2010; Roseberry et al., 2012;), normal
240 (C. Ancey & Heyman, 2014; Heyman & Ancey, 2014; Martin et al., 2012), Gamma (Liu et al., 2019), lognormal
241 (Shim & Duan, 2019) and alpha stable distribution with power law tails (Zhu et al., 2019). To the best of our
242 knowledge, only (Salevan et al., 2017) modelled the PDF for all the motion states, proposing the following bimodal
243 distribution:

$$f(u \mid A, \sigma, \xi, \mu_u) = A f_1(u \mid \sigma, \xi) + (1 - A) f_2(u \mid \mu_u) \tag{8}$$

where:

$$f_1(u^{NT} \mid \sigma, \xi) = \frac{\Gamma\left(\frac{\xi+1}{2}\right)}{\sigma\sqrt{\xi\pi}\,\Gamma\left(\frac{\xi}{2}\right)} \left(\frac{\xi + \left(\frac{u^{NT}}{\sigma}\right)^2}{\xi} \right)^{-\frac{\xi+1}{2}} \tag{9}$$

$$f_2(u^{T} \mid \mu_u) = \frac{1}{\mu_u} \exp - \frac{u^{T}}{\mu_u} \tag{10}$$

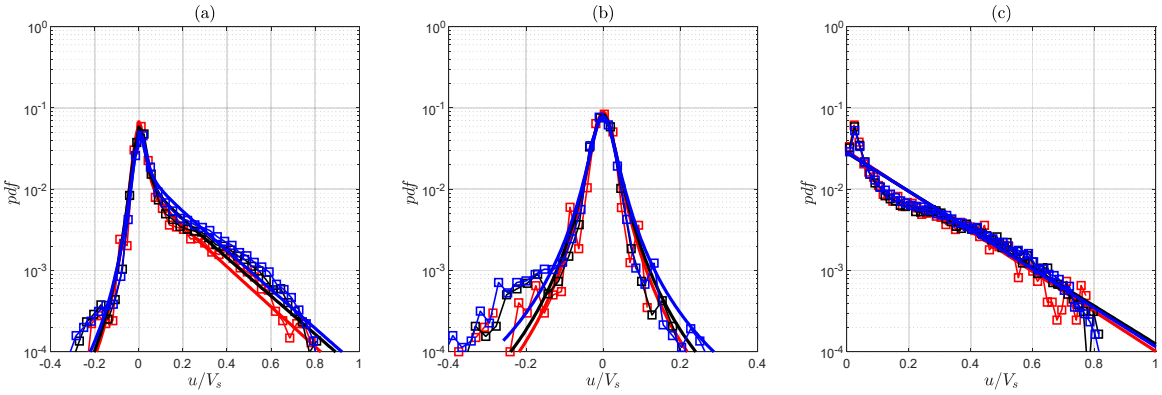

Fig. 6 Probability distribution function of the instantaneous velocity u: (a) all motion; (b) NT state; (c) T state. For all the panels: $u_*/u_{*c} = 1.11$ (red), $u_*/u_{*c} = 1.22$ (black) and $u_*/u_{*c} = 1.30$ (blue). Continuous lines represent the theoretical PDFs (Eqn. 8-10), while squares are for the experimental ones. For $u_*/u_{*c} = 1.11$: $A = 0.63;\ \sigma = 4.04; \xi = 2.64; \mu_u = 34.12$. For $u_*/u_{*c} = 1.22$: $A = 0.56;\ \sigma = 4.36; \xi = 2.51; \mu_u = 35.72$. For $u_*/u_{*c} = 1.30$: $A = 0.45;\ \sigma = 4.51; \xi = 2.12; \mu_u = 35.10$.

This model is composed by two terms describing the behaviour of the NT (f_1) and T states (f_2). We calibrated the parameters of (8) considering all the moving particles. Fig. 6(a) shows a satisfactory comparison between the experimental PDF and the theoretical distribution. In the caption we report the calibrated parameters: the values of

254 μ_u are consistent with those of (Salevan et al., 2017); the other parameters are different but trends are preserved (for
255 increasing u_*/u_{*c}, σ and A increase, while ξ decreases). The detected discrepancy may be due to the many small
256 displacements considered by (Salevan et al., 2017); in fact, the peak of their distribution was one order of magnitude
257 bigger that that showed in Fig. 6(a). We remark that in this work many small displacements have been filtered out
258 by the thresholds δr_t and δd_t; in addition, our frame rate is smaller than that of Salevan et al. (32 vs 250 fps), thus
259 causing additional filtering.

260 In their work, (Salevan et al., 2017) did not propose any criteria for the distinction between the T and NT states. In
261 contrast, in this manuscript we did so, and thus we were able to obtain the experimental PDF of the particle velocity
262 for both states. Without any further calibration, in Fig. 6 (b) and (c) we compare the experimental and the theoretical
263 distributions of the two states, separately. The agreement is satisfactory, even though the experimental PDF for the
264 NT state is slightly skewed left.

265 4.4 Contribution of the motion states to bulk variables

266 We present and discuss the effect of the two states on four significant bulk variables using Tab. 1, where we report
267 the values of: the cumulative number of particles that crossed a reference transverse line ΣN_Q; the mean kinetic
268 energy per unit mass, $\bar{k}$; the mean number of moving particles, $\overline{N}^m$; and the mean stream-wise velocity, $\bar{u}$. The
269 values are provided considering the motion states together and for the T and NT states separately, finally computing
270 the relative contributions for the states.

271 Considering both motion states, all the variables increase for increasing shear velocity, as expected. The values
272 obtained separating the T and NT states show that the latter has negligible contribution to ΣN_Q, generalizing the
273 results of Fig. 4(a). By contrast, the contribution of the NT state to the kinetic energy is not negligible as, for our
274 experiments, it is around 10%, with higher percentage for the weakest flow conditions.
275

276 **Tab. 1.** Cumulative number of particles that crossed the reference line, ΣN_Q. Mean values of kinetic energy per unit
277 mass, $\bar{k}$ (mm^2/s^2), number of moving particles, $\bar{N}^m$, and particle velocity, $\bar{u}$ (mm/s).

u_*/u_{*c}	T + NT	T	NT	T/(T + NT)	NT/(T + NT)
ΣN_Q					
1.11	6	6	0	100%	0%
1.22	37	37	0	100%	0%
1.30	96	99	-3	103%	-3%
$\bar{k}$					
1.11	2901	2549	352	88%	12%
1.22	14773	13462	1311	91%	9%
1.30	28127	26263	1864	93%	7%
$\bar{N}^m$					
1.11	5.45	2.53	2.92	47%	53%
1.22	21.24	11.92	9.33	56%	44%
1.30	34.73	22.63	12.09	65%	35%
$\bar{u}$					
1.11	12.67	28.24	-0.85		
1.22	16.07	29.77	-1.43		
1.30	19.52	31.04	-2.03		

278

279 We now focus on two primary variables determining the sediment transport rate, namely, the number of moving
280 particles and the particle stream-wise velocity. The number of moving particles increases with transport intensity,
281 for both the T and NT states, but the relative contribution of the NT state decreases. The average velocity for the T
282 state is much larger than the average for both states, because $\bar{u}^{NT}$ is close to zero (and, moreover, negative in the

present experiments). The mean velocity $\bar{u}^T$ increases for increasing u_*, but much less than linearly; a low increasing rate of particle velocity close to the threshold condition has been previously reported by, for example, (Ali & Dey, 2019). The increase of $\bar{u}^{T+NT}$ with u_* is stronger, but this is due to the fact that, for progressively higher shear velocity, the proportion of the NT state is smaller, as previously mentioned.

With a small increase of shear velocity, the sediment transport rate increases by one order of magnitude, this being mostly due to the increase of $\overline{N^m}$ (both for the T state and for all the moving states), consistently with the findings of (Radice & Ballio, 2008). In addition, the contribution of the NT state to the sediment transport rate is negligible because the average $\bar{u}^{NT}$ is close to zero.

4.5 Discussion

The separation between the T and NT states of motion is a tricky part of any analysis of sediment kinematics. The criterion used in the present manuscript, once biases possibly induced by experimental uncertainties are properly removed, does not depend on any threshold to be chosen by a user. Furthermore, it is based on instantaneous conditions and not on, for example, integrated displacements or durations of resting times. Our criterion also has some limitations, related to being restricted to the stream-wise particle position (a generalization to more complex motion might not be straightforward), and unable to recognize the particle state at the first instant in which a particle is observed, because information about the particle at previous time instants is obviously unavailable (thus, if a particle track starts with a forward movement, this is always labelled as in T state,. However, application of filter (2) reasonably returns the expected phenomenology of the two states: downstream mass transport (state T) and isotropic vibration (state NT).

Furthermore, Fig. (5) demonstrates the existence of a transition zone where the histograms of u for the T and NT states overlap. As a consequence, any sediment transport variable can be affected by the criteria used for the distinction between T and NT particles (as demonstrated, for example, for hop length by (Hosseini-Sadabadi et al., 2019)). Some authors distinguished the states of stillness and motion imposing a cutoff stream-wise velocity (Heyman & Ancey, 2014; Lajeunesse et al., 2010; Roseberry et al., 2012). Since imposing a threshold on particle velocity is equivalent to separating states based on a vertical line in Fig. (5), it inevitably induces some bias in the state separation. The experimental probability distributions obtained in the present work are in satisfactory agreement with the theoretical model of Salevan et al. (2017); it is noticeable that, once the model parameters were

calibrated for the distributions of all the velocity values, the individual distributions for the T and NT states were also well represented.

After doing the exercise of separating motions in T and NT state, one can judge if the separation is worth being performed. In our opinion, from a phenomenological point of view, separation is worth, as it increases the richness of our depiction of the process. Quantitatively, we have demonstrated that the inclusion of the NT state significantly affects the primary variables $\overline{\mathrm{N}^{\mathrm{m}}}$ and $\bar{\mathrm{u}}$. If the primary purpose of a study is the determination of the sediment transport rate, the NT state can be considered disregarded (that is, considered as stillness); alternatively, we suggest to exclude such state from the computation of mean values, since it does not contribute to mass transport. Vice-versa, if one is interested on the kinetic energy associated to particle motion, the NT state should be either considered as motion (not distinguishing T and NT) or appropriately accounted for in the determination of the energy budget.

5 Conclusions

In this paper, we conceptualized bed-load particle motion using three states: stillness, transport (T) and non-transport (NT). With reference to recent laboratory experiments, we tracked individual particles, quantified experimental errors introducing objective filters and finally proposed one-dimensional, instantaneous and non-parametric criteria for distinguishing the different states.

The main conclusions of this work are:

- The proposed criteria clearly allow a distinction between different phenomena: particles whose mass is transported downstream and particles that fluctuate without a neat contribution to mass transport.
- The histograms of the stream-wise sediment velocity for the T and NT states partially overlap, thus the two states cannot be separated by criteria based on just a cut-off velocity value.
- If one fits a theoretical probability distribution to the entire velocity sample, then the distributions for the T and NT states separately are represented satisfactorily.

- Accounting or not accounting for the values for NT state changes the mean values of variables of interest for the bed-load process (number of moving particles, particle velocity, sediment transport rate, sediment kinetic energy).
- The separation between the T and NT states is worth from a phenomenological point of view. Depending on what one is interested in, inclusion of the NT state in the computation of mean values can be more or less appropriate. Particularly, we recommend to exclude the data for the NT state when determining the sediment transport rate.

Acknowledgments

The present research has been financially supported by the Italian Ministry of University and Research, that funded the Ph.D. scholarship of D.R.

Open Research

The particle's trajectories used in the study are available at zenodo.org via the following DOI: https://doi.org/10.5281/zenodo.7849873.

Notation

A	=	model parameter;
a_x	=	instantaneous particle x-acceleration;
a_y	=	instantaneous particle y-acceleration;
d	=	sediment size;
g	=	acceleration due to gravity;
k	=	particle kinetic energy per unit mass;
M^m	=	clipping function for the motion state;
M^s	=	clipping function for the still state;
M_Q	=	clipping function for the particles crossing a specific line;
N^m	=	number of particle in motion state at time t;
N_Q	=	number of particles that crossed a specific line at time t;

u = instantaneous particle x-velocity;

u_* = shear velocity;

u_{*c} = critical shear velocity;

v = instantaneous particle y-velocity;

V = velocity magnitude;

V_s = characteristic settling velocity ($V_s = \sqrt{g\Delta d}$);

x = stream-wise coordinate;

x_* = transversal line where mass transport is measured;

X^T = any variable related to the transported particles;

X^{NT} = any variable related to the non-transported particles ;

$\overline{X}$ = any variable averaged in time;

y = transversal coordinate;

α = instantaneous direction;

δd = change of the measured diameter between two consecutive frames;

δd_t = threshold for spot diameter change;

δr = instantaneous displacement;

δr_t = minimum measurable displacement;

δt = small time interval;

δx = instantaneous x-displacement;

δy = instantaneous y-displacement;

Δ = sediment density ratio ($\Delta = (\rho_g-\rho)/\rho$);

μ = water viscosity;

θ = Shields number $\theta = u_*^2 / g\Delta d_{50}$;

θ_c = threshold Shields number;

μ_u = model parameter;

ξ = model parameter;

ρ = water density;

ρ_s = sediment density;

σ = model parameter;

σ_g = sediment uniformity coefficient;

References

Ali, S. Z., & Dey, S. (2019). Bed particle saltation in turbulent wall-shear flow: A review. *Proceedings of the Royal Society A: Mathematical, Physical and Engineering Sciences*, *475*(2223). https://doi.org/10.1098/rspa.2018.0824

Ancey, C., Davison, A. C., Böhm, T., Jodeau, M., & Frey, P. (2008). Entrainment and motion of coarse particles in a shallow water stream down a steep slope. *Journal of Fluid Mechanics*, *595*, 83–114. https://doi.org/10.1017/S0022112007008774

Ancey, C., & Heyman, J. (2014). A microstructural approach to bed load transport: Mean behaviour and fluctuations of particle transport rates. *Journal of Fluid Mechanics*, *744*, 129–168. https://doi.org/10.1017/jfm.2014.74

Ancey, Christophe, Böhm, T., Jodeau, M., & Frey, P. (2006). Statistical description of sediment transport experiments. *Physical Review E - Statistical, Nonlinear, and Soft Matter Physics*, *74*(1), 1–14. https://doi.org/10.1103/PhysRevE.74.011302

Ballio, F., Nikora, V., & Coleman, S. E. (2014). On the definition of solid discharge in hydro-environment research and applications. *Journal of Hydraulic Research*, *52*(2), 173–184. https://doi.org/10.1080/00221686.2013.869267

Ballio, F., Pokrajac, D., Radice, A., & Hosseini Sadabadi, S. A. (2018). Lagrangian and Eulerian Description of Bed Load Transport. *Journal of Geophysical Research: Earth Surface*, *123*(2), 384–408. https://doi.org/10.1002/2016JF004087

Böhm, T., Ancey, C., Frey, P., Reboud, J. L., & Ducottet, C. (2004). Fluctuations of the solid discharge of gravity-

driven particle flows in a turbulent stream. *Physical Review E - Statistical Physics, Plasmas, Fluids, and Related Interdisciplinary Topics*, *69*(6), 13. https://doi.org/10.1103/PhysRevE.69.061307

Campagnol, J. (2012). *Characterization of bed load sediment transport at the grain scale*. Politecnico di Milano.

Campagnol, J., Radice, A., Ballio, F., & Nikora, V. (2015). Particle motion and diffusion at weak bed load: Accounting for unsteadiness effects of entrainment and disentrainment. *Journal of Hydraulic Research*, *53*(5), 633–648. https://doi.org/10.1080/00221686.2015.1085920

Campagnol, J., Radice, A., Nokes, R., Bulankina, V., Lescova, A., & Ballio, F. (2013). Lagrangian analysis of bed-load sediment motion: Database contribution. *Journal of Hydraulic Research*, *51*(5), 589–596. https://doi.org/10.1080/00221686.2013.812152

Cecchetto, M., Tregnaghi, M., Bottacin-Busolin, A., Tait, S. J., Cotterle, L., & Marion, A. (2018). Diffusive Regimes of the Motion of Bed Load Particles in Open Channel Flows at Low Transport Stages. *Water Resources Research*, *54*(11), 8674–8691. https://doi.org/10.1029/2018WR022885

Charru, F., Mouilleron, H., & Eiff, O. (2004). Erosion and deposition of particles on a bed sheared by a viscous flow. *Journal of Fluid Mechanics*, *519*, 55–80. https://doi.org/10.1017/S0022112004001028

Einstein, H. A. (1950). *The bed-load function for sediment transportation in open channel flows.*

Fan, N., Singh, A., Guala, M., Foufoula-Georgiou, E., & Wu, B. (2016). Exploring a semimechanistic episodic Langevin model for bed load transport: Emergence of normal and anomalous advection and diffusion regimes. *Journal of the American Water Resources Association*, *52*, 2789–2801. https://doi.org/10.1002/2015WR018023

Fathel, S. L., Furbish, D. J., & Schmeeckle, M. W. (2016). *Journal of Geophysical Research : Earth Surface Experimental evidence of statistical ensemble behavior in bed load sediment transport*. 2298–2317. https://doi.org/10.1002/2015JF003552.Received

Furbish, D. J., Haff, P. K., Roseberry, J. C., & Schmeeckle, M. W. (2012). A probabilistic description of the bed load sediment flux: 1. Theory. *Journal of Geophysical Research: Earth Surface*, *117*(3). https://doi.org/10.1029/2012JF002352

González, C., Richter, D. H., Bolster, D., Bateman, S., Calantoni, J., & Escauriaza, C. (2017). Characterization of bedload intermittency near the threshold of motion using a Lagrangian sediment transport model. *Environmental Fluid Mechanics*, *17*(1), 111–137. https://doi.org/10.1007/s10652-016-9476-x

435 Heays, K. G., Friedrich, H., Melville, B. W., & Nokes, R. (2014). Quantifying the Dynamic Evolution of Graded
436 Gravel Beds Using Particle Tracking Velocimetry. *Journal of Hydraulic Engineering*, *140*(7), 2–10.
437 https://doi.org/10.1061/(asce)hy.1943-7900.0000850
438 Heyman, J., & Ancey, C. (2014). Tracking bed load particles in a steep flume: Methods and results. *Proceedings of*
439 *the International Conference on Fluvial Hydraulics, RIVER FLOW 2014*, 909–916.
440 https://doi.org/10.1201/b17133-123
441 Hosseini-Sadabadi, S. A., Radice, A., & Ballio, F. (2019). On Reasons of the Scatter of Literature Data for Bed-
442 Load Particle Hops. *Water Resources Research*, *May 2018*. https://doi.org/10.1029/2018WR023350
443 Kalinske, A. A. (1947). Movement of sediment as bed-load in rivers. *Trans Am Geophys Union*, *28*(4), 615–620.
444 Lajeunesse, E., Malverti, L., & Charru, F. (2010). Bed load transport in turbulent flow at the grain scale:
445 Experiments and modeling. *Journal of Geophysical Research: Earth Surface*, *115*(4).
446 https://doi.org/10.1029/2009JF001628
447 Liu, M. X., Pelosi, A., & Guala, M. (2019). A Statistical Description of Particle Motion and Rest Regimes in Open-
448 Channel Flows Under Low Bedload Transport. *Journal of Geophysical Research: Earth Surface*, *124*(11),
449 2666–2688. https://doi.org/10.1029/2019JF005140
450 Martin, R. L., Jerolmack, D. J., & Schumer, R. (2012). The physical basis for anomalous diffusion in bed load
451 transport. *Journal of Geophysical Research: Earth Surface*, *117*(1), 1–18.
452 https://doi.org/10.1029/2011JF002075
453 Nikora, V., Habersack, H., Huber, T., & McEwan, I. (2002). On bed particle diffusion in gravel bed flows under
454 weak bed load transport. *Water Resources Research*, *38*(6), 17-1-17–19.
455 https://doi.org/10.1029/2001wr000513
456 Nikora, V., Heald, J., Goring, D., & McEwan, I. (2001). Diffusion of saltating particles in unidirectional water flow
457 over a rough granular bed. *Journal of Physics A: Mathematical and General*, *34*(50).
458 https://doi.org/10.1088/0305-4470/34/50/103
459 Nokes, R. (2012). *Streams v. 2.00. System theory and design*.
460 Radice, A., & Ballio, F. (2008). Double-average characteristics of sediment motion in one-dimensional bed load.
461 *Acta Geophysica*, *56*(3), 654–668. https://doi.org/10.2478/s11600-008-0015-0
462 Radice, A., Sarkar, S., & Ballio, F. (2017). Image-based Lagrangian particle tracking in bed-load experiments.

Journal of Visualized Experiments, *2017*(125), 1–11. https://doi.org/10.3791/55874

Roseberry, J. C., Schmeeckle, M. W., & Furbish, D. J. (2012). A probabilistic description of the bed load sediment flux: 2. Particle activity and motions. *Journal of Geophysical Research: Earth Surface*, *117*(3). https://doi.org/10.1029/2012JF002353

Salevan, J. C., Clark, A. H., Shattuck, M. D., O'Hern, C. S., & Ouellette, N. T. (2017). Determining the onset of hydrodynamic erosion in turbulent flow. *Physical Review Fluids*, *2*(11), 1–11. https://doi.org/10.1103/PhysRevFluids.2.114302

Sechet, P., & Le Guennec, B. (1999). The role of near wall turbulent structures on sediment transport. *Water Research*, *33*(17), 3646–3656. https://doi.org/10.1016/S0043-1354(99)00072-X

Seizilles, G., Lajeunesse, E., Devauchelle, O., & Bak, M. (2014). Cross-stream diffusion in bedload transport. *Physics of Fluids*, *26*(1). https://doi.org/10.1063/1.4861001

Shim, J., & Duan, J. (2019). Experimental and theoretical study of bed load particle velocity. *Journal of Hydraulic Research*, *57*(1), 62–74. https://doi.org/10.1080/00221686.2018.1434837

Shim, J., & Duan, J. G. (2017). Experimental study of bed-load transport using particle motion tracking. *International Journal of Sediment Research*, *32*(1), 73–81. https://doi.org/10.1016/j.ijsrc.2016.10.002

Wu, Z., Furbish, D., & Foufoula-Georgiou, E. (2020). Generalization of Hop Distance-Time Scaling and Particle Velocity Distributions via a Two-Regime Formalism of Bedload Particle Motions. *Water Resources Research*, *56*(1), 1–14. https://doi.org/10.1029/2019WR025116

Zhu, Z., Zhang, S., & Chen, D. (2019). Statistical analysis of bed load transport over an armored bed layer with cluster microforms. *Water (Switzerland)*, *11*(10). https://doi.org/10.3390/w11102082